Int. J. Heat Mass Transfer. Vol. 5, pp. 837–857. Pergamon Press 1962. Printed in Great Britain.

THEORETICAL ANALYSIS OF THE DOWNSTREAM INFLUENCE OF MASS TRANSFER IN A STAGNATION REGION

ROBERT J. CRESCI
Polytechnic Institute of Brooklyn

(*Received* 11 *August* 1961 *and in revised form* 19 *January* 1962)

Abstract—The integral method has been applied to determine the downstream influence of homogeneous mass transfer in the stagnation region of a blunt, axisymmetric body under hypersonic flight conditions. Exponential profiles are employed in an attempt to eliminate singularities which have appeared in previous analyses utilizing polynomial profiles. The analysis is performed by introducing an additional differential equation, obtained by a second integration of the momentum equation. When used in conjunction with the von Kármán integral relations for the momentum and energy equations a system of first-order differential equations result which are solved by numerical means on a digital computer. The matching conditions at the junction of the permeable–impermeable surface provide the initial conditions for the integration.

The results indicate that the singularities occurring in the application of the integral method using polynomial profiles do not arise in the present analysis. The heat-transfer rates obtained are compared to experimental data and are found to predict the downstream effect of the mass injection reasonably well. The effect, on the heat-transfer rates, of varying the coolant temperature and the injection area are also investigated. It is found that decreasing the coolant temperature or increasing the injection area result in a decrease in the peak heat rate and over-all heat transferred to the body.

NOMENCLATURE

a_1 $= 0{\cdot}5 + 0{\cdot}25K_1$;
a_2 $= 0{\cdot}75 + 0{\cdot}25K_1$;
a_3 $= 1{\cdot}75 + 0{\cdot}375K_1$;
a_4 $= -0{\cdot}625 + 1{\cdot}25K_1 + 0{\cdot}4375K_1^2$;
a_5 $= 1{\cdot}25 + 1{\cdot}25K_1$;
a_6 $= 0{\cdot}5 - K_1 - 0{\cdot}5K_1^2$;
C $\equiv (\rho\mu)/\rho_e\mu_e$, mass density–viscosity ratio;
f_w, non-dimensional mass injection rate;
$\bar{H}$ $= \psi^*/\psi$, modified form factor;
H_c $\equiv \delta^*/\theta$, form factor;
h_s, stagnation enthalpy;
I $= \left\{\int_0^\infty \left(\frac{h_s}{h_{s_e}}\right)^{n-1}\left(\frac{u}{u_e}\right)_t \mathrm{d}\left(\frac{t}{\lambda}\right)\right\}_{\bar{x}-\Delta\bar{x}}$;
K_1, coefficient in velocity profile defined by equation (7);
K_2, K_3, coefficients in enthalpy profile defined by equation (8);
m_c, mass flow per unit time of injected gas;
N_1 $= m_c/R_0\mu_{s_e}\tilde{N}_R^{\frac{1}{2}}$, mass transfer similarity parameter;
N_{Nu} $= q_wC_{p_{s_e}}R_0/(h_{s_e} - h_w)k_{s_e}$, Nusselt number;
$\tilde{N}_R$ $= [\rho_{s_e}\sqrt{(h_{s_e})}\,R_0/\mu_{s_e}]\,\varphi_{s_e}^{\frac{1}{2}}$;
n, exponent in viscosity–enthalpy ratio $(\mu/\mu_e) = (h_s/h_{s_e})^n$;
Q, effective enthalpy [defined by equation (28)];
q, heat transfer per unit area per unit time;
R_0, nose radius;
r, radial co-ordinate from center line of symmetry to surface;
$\bar{r}$ $= r/R_0$;
T, temperature;
T_w, coolant temperature;
t, $= \int_0^y (\rho\mu_{s_e})/(\rho_e\mu_e)\,\mathrm{d}y$, transformed normal co-ordinate;
u, velocity component parallel to surface;
$\bar{u}$ $= u_e/\sqrt{(h_{s_e})}$, non-dimensionalized velocity component parallel to the surface;

W $\equiv h_w/h_{s_e}$ impermeable surface enthalpy ratio;
x, surface co-ordinate;
$\bar{x}$ $= x/R_0$, non-dimensionalized surface co-ordinate;
y, co-ordinate normal to the surface;
β $= \mathrm{d}\bar{u}/\mathrm{d}\bar{x}$, non-dimensional velocity gradient along the surface;
Γ $= 1 - K_1 - 0{\cdot}5K_1^2$;
δ^* $\equiv \int_0^\infty \left(1 - \frac{u}{u_e}\right) \mathrm{d}t$, displacement thickness;
θ $\equiv \int_0^\infty \frac{u}{u_e}\left(1 - \frac{u}{u_e}\right) \mathrm{d}t$, momentum thickness;
θ_w $\equiv T_w/T_e$, porous wall temperature ratio;
Λ $\equiv \Omega/\theta$ shape factor;
λ, parameter in velocity and enthalpy profiles;
$\bar{\lambda}$ $= \lambda \tilde{N}_R^{\frac{1}{2}}/R_0\varphi_{s_e}^{\frac{1}{2}}$;
μ, viscosity coefficient;
ρ, mass density;
σ, Prandtl number;
τ $= \int_0^t \frac{u}{u_e}\mathrm{d}t$;
Φ, modified momentum thickness defined by equation (16);
Φ^*, modified displacement thickness defined by equation (17);
φ_1 $= a_1 + a_2 K_3 + a_3 K_2$;
φ_2 $= a_2 + a_3 + (1 - n)(1 - W)(1 - K_3)/W$;
φ_3 $= 0{\cdot}25 + 0{\cdot}25K_3 + 0{\cdot}375K_2$;
φ_{s_e} $= p_{s_e}/\rho_{s_e}h_{s_e}$, real gas parameter;
ψ $= \int_0^\infty \Phi \, \mathrm{d}t$;
ψ^* $= \int_0^\infty \Phi^* \, \mathrm{d}t$;
Ω $\equiv \int_0^\infty \frac{u}{u_e}\left(1 - \frac{h_s}{h_{s_e}}\right) \mathrm{d}t$, energy thickness.

Subscripts

e, conditions external to the boundary layer;
i, conditions evaluated at the termination of the injection region;
s, denotes stagnation conditions;
s_e, stagnation conditions external to the boundary layer;
T, denotes maximum length of surface influenced by the coolant;
w, conditions evaluated at the surface, $y = 0$;
$\overline{(\ )}$, quantities non-dimensionalized with respect to external conditions;
$(\ )_t$ $= \partial/\partial t$, denotes partial differentiation with respect to the transformed normal co-ordinate;
$(\ )_x$ $= \partial/\partial x$ denotes partial differentiation with respect to the surface co-ordinate.

I. INTRODUCTION

MASS-TRANSFER cooling has been shown to provide an efficient means of reducing the surface temperature of high-speed flight vehicles to tolerable structural limits. Since the injection region is porous, its structural characteristics are in general inferior to those of an impermeable surface; as a result, it is desirable to localize the region in which the coolant is injected into the stream. From the viewpoint of aerodynamic heating, the regions of peak heat rate can be effectively reduced by the insertion of a porous strip in the required location. For blunt-nosed hypersonic bodies, the most efficient location for the injection region is at the forward stagnation point. The heat transfer is thereby reduced in the region corresponding to maximum heating; moreover, the favorable effect of the injected gas will persist for some distance downstream of the injection region. This persistence is advantageous from the viewpoint of coolant economy as well as over-all effectiveness.

The problem considered here is the determination of the boundary-layer characteristics downstream of the region of mass transfer. The effects of variation of coolant temperature and spatial extent of mass injection are also studied. As a fundamental hypersonic body, a hemisphere cylinder is used for the analysis. The impermeable surface temperature, coolant temperature, and injection area for one computed case are chosen to correspond to an experimental model for which data on the downstream surface are available.

Although there is extensive literature for the determination of the laminar boundary layer on a permeable surface, similar information is

relatively scarce for the impermeable surface downstream of the mass-transfer region. For the porous region, Morduchow [1] has studied the case of homogeneous injection over a surface with arbitrary pressure gradient by means of the integral method. Livingood and Donoughe [2] present a summary of transpiration cooling problems based on similar solutions. These solutions are applicable to wedge-type flows over two-dimensional surfaces, and include solutions valid over a range of Prandtl numbers and for variable transport properties. Howe and Mersman [3] extend these solutions to include the stagnation region of an axially symmetric body.

Libby [4] also treats the homogeneous mass-transfer problem for an axisymmetric stagnation region with large rates of injection. Solutions are presented for a wide variation of injection rates, extending well into the regime in which the heat transfer to the porous region is identically zero. At present, these are the only results adaptable to the problem considered herein. Since most of the other literature concerning the porous region has its interest directed only to the reduction of heat transfer on the injection region itself, relatively low rates of mass transfer were used. To attain a large reduction downstream of the transpiration cooled portion, however, much higher rates of mass transfer are expected to be applicable.

Consider now the downstream region; Howe [5] has solved the problem of a flat plate with homogeneous upstream injection by means of a finite-difference method and compared the results with those of Libby and Pallone [6] and of Rubesin and Inouye [7]. Both [6] and [7] are based on the integral method, the differences being mainly in the method by which the injection profiles and impermeable region profiles are joined. In [6] additional parameters were used in the profiles to insure the continuity of mass, momentum and energy in the boundary layer. These parameters, however, were assumed to be constant instead of functions of the surface co-ordinate, and, as a result, the analysis is not valid when the distance from the injection region is large. In [7] the profiles were matched by assuming the shear stress and boundary-layer thickness to be continuous at the junction. In comparing the results of [6] and [7], only the overall effects of the two methods could be evaluated; there is no way of determining the validity of the individual assumptions considered. Chung [8] treats the problem of downstream influence for low injection rates over a blunt two-dimensional or axisymmetric body utilizing the hypersonic approximations of Lees [9]. The solution presented corresponds to the "cold wall" condition wherein the pressure gradient term in the momentum equation is neglected. The boundary-layer profiles and matching conditions are the same as those of [7]. Pallone [10] presents a method which involves a more complex system of equations but provides more accurate results than the usual integral method. It consists of dividing the boundary layer into strips and integrating the pertinent equations from the wall to the edge of each strip. The results of this analysis for the downstream influence of mass transfer on a flat plate are substantially the same as those of [5].

In this report, the effects on the boundary-layer of injecting a gas in the stagnation region of a blunt, axisymmetric body are considered. The profiles of Libby [4] are utilized on the porous region while the impermeable region is treated by application of the integral method using exponential profiles.

Previous experience with polynomial profiles in flows with favorable pressure gradient and moderate rates of heat transfer indicated the appearance of singularities in the solution of the resulting integral equations of momentum and energy (cf. [11] and [12]). These singularities arise when the density at the wall is approximately equal to that in the external stream, and do not appear when "cold wall" conditions exist; moreover, the singularities correspond to non-monotonic velocity profiles. In an attempt to circumvent the possible appearance of these singularities, exponential profiles were utilized rather than the more usual polynomials. Lew [13] found that, for large rates of suction in a compressible boundary layer over a flat plate, polynomial profiles led to singularities which could be avoided by the use of exponential profiles. It should be noted that, if the actual boundary layer behavior corresponds to non-monotonic profiles (e.g. [2] and [14]), the exponential profiles can represent them satisfactorily.

The applicability of the integral method in analysing a laminar hypersonic boundary layer over a blunt body has been indicated by Libby [12]. In order to determine the accuracy that could be expected in the prediction of heat transfer with mass injection, the method of the present study using exponential profiles was applied under the same conditions as [12]. A completely impermeable body was used and the results of the present analysis were compared to those of [12] as well as those of more exact methods. Fay and Riddell [15] have obtained an accurate relation for the stagnation-point heat transfer and Lees [9] has presented a method for obtaining the corresponding surface distribution. In [9] the assumptions utilized are the existence of a cold wall and a constant value of the density–viscosity ratio across the boundary layer. In previous applications of the integral method using polynomial profiles, this latter assumption appears to be unavoidable. Use of exponential profiles, however, seems to circumvent this obstacle and permit the product $\rho\mu$ to remain variable in the analysis. Kemp *et al.* [16] extended the analysis of [15] under the assumptions of equilibrium in the boundary layer and local similarity. This solution, when compared with [9] indicated that the results of Lees were very accurate, notwithstanding the assumption of constant $\rho\mu$. As a result, the present analysis will be compared to the surface distribution predicted by Lees with the stagnation-point value taken to be that of Fay and Riddell. This procedure has been found to be in good agreement with experiment for a wide variety of body geometries (cf. [17] and [18]).

After the relative accuracy has been thus established, the basic problem of determining the downstream effect of stagnation-point mass transfer is treated. This reduces to solving a system of simultaneous algebraic and differential equations subject to specified initial conditions. The differential equations resulting from the integral representation of the momentum and energy equations are of first order, therefore they are readily solved by numerical means. A modified Runge–Kutta method [19] was used and the equations were subsequently solved on a Bendix G-15 digital computer.

II. BASIC EQUATIONS AND DEVELOPMENT OF METHOD

The equations used in the analysis describe the laminar compressible boundary-layer flow over an axisymmetric unyawed, blunt body. The fluid is assumed to be in thermodynamic equilibrium, with a Lewis number of unity. The Prandtl number is constant, although its value can be different from unity. Utilizing the boundary conditions for the impermeable surface and the continuity equation to eliminate the normal component of velocity, the momentum and energy equations can be integrated across the boundary layer and result in the standard form of the von Kármán integral equations. Since the profiles to be used in the solution of these equations are exponential, the integration limit extends to infinity and the usual assumption of a single boundary-layer thickness is unnecessary.

Using a modified Dorodnitzin transformation of the co-ordinate normal to the surface, the following form of the momentum and energy equations result (cf. [6] and [12]):

$$\frac{\mathrm{d}\theta}{\mathrm{d}x} + \theta \frac{\mathrm{d}}{\mathrm{d}x} \ln (\rho_e \mu_e r) + \frac{\theta}{u_e} (H_c + 2) \frac{\mathrm{d}u_e}{\mathrm{d}x} = \frac{\mu_{s_e}^2 [C(u/u_e)_t]_w}{\rho_e u_e \mu_e} \quad (1)$$

$$\frac{\mathrm{d}\Omega}{\mathrm{d}x} + \Omega \frac{\mathrm{d}}{\mathrm{d}x} \ln (\rho_e \mu_e u_e r) = \frac{\mu_{s_e}^2 [C(h_s/h_{s_e})_t]_w}{\rho_e \mu_e u_e} \quad (2)$$

where the transformed normal co-ordinate t is related to the physical co-ordinate y by

$$\mathrm{d}t = \frac{\rho \mu_{s_e}}{\rho_e \mu_e} \mathrm{d}y \quad (3)$$

and the integral thicknesses in the t-plane are as follows:

momentum thickness

$$\theta = \int_0^\infty \frac{u}{u_e} \left(1 - \frac{u}{u_e}\right) \mathrm{d}t, \quad (4)$$

displacement thickness

$$\delta^* = \int_0^\infty \left(\frac{\rho_e}{\rho} - \frac{u}{u_e}\right) \mathrm{d}t, \quad (5)$$

energy thickness

$$\Omega = \int_0^\infty \frac{u}{u_e}\left(1 - \frac{h_s}{h_{s_e}}\right) \mathrm{d}t. \qquad (6)$$

The profiles chosen correspond to velocity and stagnation enthalpy distributions in the boundary layer. With the thermodynamic and transport properties related to the local flow variables, the equations are in a form suitable for solution. If the degree of dissociation in the boundary layer is small, approximate relations can be found; these are reasonably accurate for stagnation temperatures less than 5000°R. These expressions relate the enthalpy, specific heat and viscosity to the local temperature by means of a power-law variation. This approach has previously been used in [3, 4, 20]. Since the profiles of [4] are used as initial conditions on the present analysis, the exponents involved in these relationships correspond to those of [4], with a slight modification. In the notation of [4] the thermodynamic and transport properties of interest are related by

$$\frac{T}{T_e} = \frac{\rho_e}{\rho} = \left(\frac{\mu}{\mu_e}\right)^{1\cdot43}.$$

In the present analysis the major region of interest for cooling purposes is confined to the region where the higher heat-transfer rates prevail;† this corresponds to a region of high external pressure or low external Mach number. This results in the following relation between density and stagnation enthalpy,

$$\frac{\rho_e}{\rho} \simeq \frac{h_s}{h_{s_e}}.$$

Using this in conjunction with the density–viscosity relation, given in [4], results in

$$\frac{\mu}{\mu_e} \simeq \left(\frac{h_s}{h_{s_e}}\right)^n$$

and $C = \rho\mu/\rho_e\mu_e = (h_s/h_{s_e})^{n-1}$ where $n = 0{\cdot}7$.

Therefore, for a given set of profiles for the velocity and stagnation enthalpy, the integral thicknesses can be obtained in terms of the unknown coefficients. These coefficients are then determined as a function of the surface co-ordinate x from the integral form of the basic equations. If, as is generally the case, there are more than two independent coefficients in the velocity and enthalpy profiles, additional equations must be supplied to determine these quantities as functions of x. Various methods of obtaining these additional equations have been used in previous analyses. If the boundary-layer equations in partial differential form are successively differentiated with respect to y and evaluated at the wall, there result ordinary differential equations. These can be used to relate the x-wise variation of the additional parameters in the profiles. Alternatively (cf. [21]), the boundary-layer equations can be multiplied by u^m or by y^n and integrated from zero to infinity to form additional integral conditions. An analysis using the velocity as the multiplying factor has been carried out in [21], indicating, in general, a closer approximation to the exact solutions than those in which only the von Kármán integral relation was used. Whitehead [22] suggests another possible method for obtaining additional equations. This is achieved by the successive integration of the momentum equation. For an incompressible fluid, this reduces to the equation resulting from the multiplication by the normal co-ordinate and subsequent integration when combined with the von Kármán integral relation. Thus it is seen to be analogous to an equation expressing the change in the moment of momentum in the boundary layer with respect to the surface co-ordinate of the body.

In considering the profiles for the downstream region, the matching conditions at the junction of the porous surface and impermeable surface must be investigated. As discussed in [6], at this edge the boundary-layer equations are invalid inasmuch as the x-wise derivatives at the surface are infinite. However, certain integral properties of the boundary layer are usually made continuous at this station under the physically attractive assumption that within several boundary-layer thicknesses the boundary-layer approximations are again valid. The questionable validity of the boundary-layer equations at the

† The analysis can still be applied in a region of relatively large Mach number if the pressure gradient is small.

edge of a porous region can be inferred from the experimental results of [23], in conjunction with the theoretical results of [4]. In the latter, the boundary-layer thicknesses and profiles at the edge of the injection region imply zero heat transfer on the porous section. The shadowgraphs in [23] indicate a region of large density variation in the direction normal to the surface. This is explicable in terms of the profiles of [4], and indicates roughly the boundary-layer thickness. It should be noted that in a downstream distance of approximately two boundary-layer thicknesses the heat transfer determined experimentally is found to be relatively large. Such a large x-wise gradient would not appear to be consistent with the boundary-layer approximations.

Consider now the previous literature with respect to the matching conditions. In [7] the boundary-layer thickness and slope and curvature of the velocity profile at the wall are made continuous at the surface junction. Ref. [6] allows a discontinuity in the wall shear stress but specifies a continuous boundary-layer thickness as well as total mass, momentum and energy in the layer. In the finite difference analysis of [5], it is unnecessary to apply any of these assumptions explicitly. Those that are directly related to the differential equations (e.g. the wall curvature of the velocity profile) are obtained inherently as a result of the analysis. The results indicate that the skin friction and heat transfer permitted discontinuities at the interface (as stated, the discontinuous heat transfer results from the fluid motion and disregards the physical phenomenon of conduction within the body). In the present analysis the junction was treated in a manner similar to that of [6]. The specification of the continuity of mass, momentum, energy and boundary-layer thickness requires four independent parameters to be introduced into the velocity and enthalpy profiles. Moreover, in order to permit specification of arbitrary initial conditions, these must be governed by two differential equations in addition to the usual von Kármán integral relations [equations (1) and (2)].

The profiles used in this analysis, therefore, become

$$\frac{u}{u_e} = 1 - e^{-t/\lambda}\left[1 - K_1\frac{t}{\lambda}\right] \tag{7}$$

$$\frac{h_s}{h_{s_e}} = 1 - (1 - W)\,e^{-t/\lambda} \times \left[1 + K_3\frac{t}{\lambda} + K_2\left(\frac{t}{\lambda}\right)^2\right]. \tag{8}$$

The profiles involve four functions of the independent variable x, namely, λ, K_1, K_2 and K_3. All derivatives of the profiles vanish at infinity; thus it is not necessary to include the large number of terms usually required in polynomial profiles to satisfy these conditions. It is also of interest to note that the effective thicknesses of the velocity and thermal layers can be different with no difficulty; this is in contradistinction to the difficulties encountered with polynomial profiles if different thicknesses are employed in the two layers. For a Prandtl number of unity and zero pressure gradient, the parameters in equations (7) and (8) can be related by the Crocco integral; for all other cases they are independent quantities and must be determined from the differential equations.

With the profiles of equations (7) and (8), the integral thicknesses are readily obtained and result in the following:

$$\theta = \lambda\Gamma/2, \tag{9}$$

$$\delta^* = \lambda[W - K_1 - (1 - W)(K_3 + 2K_2)], \tag{10}$$

$$\Omega = \lambda(1 - W)[a_1 + a_2 K_3 + a_3 K_2]. \tag{11}$$

Consider in detail the matching conditions which result in the initial values of λ, K_1, K_2 and K_3.

The mass flow in the boundary layer can be obtained by integrating ρu across the layer. As a result of the use of exponential profiles, however, the range of integration is infinite, resulting in an infinite mass flow. It can be shown that if the difference in the mass in a layer of uniform velocity and density and the actual mass in the boundary layer is considered, a finite value is obtained which is proportional to the displacement thickness. The corresponding difference in momentum is proportional to θ and the difference in energy is proportional to Ω. From this it is seen that if the mass, momentum and energy in the boundary layer are to be

continuous, all three integral thicknesses must be continuous at the interface.

The boundary-layer thickness can be made continuous by specifying a value of u/u_e at the outer edge, since, for the exponential profiles, the velocity ratio is unity only at an infinite distance from the wall. In the present analysis, since the velocity profile is not expected to be monotonic in all cases, the boundary-layer edge is defined as the point at which

$$\left|1 - \frac{u}{u_e}\right|_\delta = 0{\cdot}02. \tag{12}$$

For those cases in which velocity overshoot occurs, the above relation is understood to designate the outermost point satisfied by the equality. The boundary-layer thickness at the junction thus provides a relation between K_1 and λ which, when used in conjunction with the integral thicknesses, determines the initial values for all the parameters. Therefore, with known profiles at the termination of the porous region (as obtained from [4], for example) the initial values of the variable coefficients in the velocity and enthalpy profiles can be determined. For the extremely large rates of injection of interest in the present analysis, however, it was found that it was not possible to satisfy the conditions simultaneously on the boundary-layer thickness and the integral thicknesses. This is a result of two separate effects; firstly, the large injection rates increase the boundary-layer thickness and integral thicknesses by a few orders of magnitude with respect to the zero injection values; and secondly, the relatively simple profiles used in the present analysis have only a limited flexibility with respect to variation of the profile parameters. The combination of these effects made it possible to satisfy all the aforementioned matching conditions only at very small injection rates.

For the results presented herein, a different method was used to determine the initial values. It was found that either the integral thicknesses or the boundary-layer thickness could be matched at the high injection rates, but not both. The boundary-layer thickness was chosen as the more desirable matching condition, since all the integral thicknesses include it as a multiplying factor. The other matching conditions are then determined from ratios of the integral thicknesses, which are independent of the boundary-layer thickness. These ratios are the form factor, $H_c \equiv \delta^*/\theta$, and shape factor, $\Lambda \equiv \Omega/\theta$. This system appears to be more reasonable than the alternate method of satisfying the integral thicknesses and not the boundary-layer thickness. Examination of the momentum thickness [equation (9)], for example, indicates the dependence of θ on two quantities, λ and Γ, where λ is proportional to the boundary-layer thickness and Γ is a quadratic function of the coefficient K_1. For real values of K_1, therefore, Γ has an upper bound. This limitation in the variation of Γ restricts the values of θ attainable for a given λ. Similar reasoning applies to δ^* and Ω, wherein the terms in the brackets [equations (10) and (11)] can vary only within specified limits. In order to insure that the same matching conditions can be applied for any combination of integral thicknesses, the form factor and shape factor are utilized. The variation of these parameters with injection rate is considerably less than the corresponding variation in integral thicknesses, since the effect of the large change in boundary-layer thickness is removed. The boundary-layer thickness itself is correctly represented since it is matched, independent of the other thicknesses.

The number of matching conditions, therefore, is reduced to three, and only three differential equations are necessary. The fourth variable is determined by satisfying the energy equation† evaluated at the wall. This results in the following:

$$\left[C_t\left(\frac{h_s}{h_{s_e}}\right)_t + C\left(\frac{h_s}{h_{s_e}}\right)_{tt} + C\left(\frac{u}{u_e}\right)_t^2(\sigma - 1)\frac{u_e^2}{h_{s_e}}\right]_w = 0$$

which reduces to a relation between the parameters in the enthalpy profile (K_3 and K_2) when

† The equation usually utilized in this connection is the momentum equation; however, the same difficulties arise in attempting to satisfy this relation as in the matching conditions at the junction. The energy equation evaluated at the surface leads to consistent results and is thus employed for the fourth equation.

either $\sigma = 1$ or $(u_e^2/h_{s_e}) \ll 1$. In terms of these variables

$$K_2 = K_3 - 0{\cdot}5 - \frac{(1-n)(1-W)}{2W}(1-K_3)^2. \quad (13)$$

Consider now the derivation of the remaining differential equation. The basic form of the momentum equation is integrated as in the von Kármán integral approach. In this case, however, the upper limit is left in terms of the normal co-ordinate y instead of being infinite. After integrating by parts and regrouping terms, the following equation is obtained:

$$\frac{1}{r}\frac{\mathrm{d}}{\mathrm{d}x}\left[ru_e^2\int_0^y \rho\left(\frac{u}{u_e}\right)^2 \mathrm{d}y - ru_e^2\frac{u}{u_e}\int_0^y \frac{\rho u}{\rho_e u_e}\,\mathrm{d}y\right] + u_e\frac{\mathrm{d}u_e}{\mathrm{d}x}\left[\int_0^y \rho_e\,\mathrm{d}y - \frac{u}{u_e}\int_0^y \rho\frac{u}{u_e}\,\mathrm{d}y\right] - u_e^2\left(\frac{u}{u_e}\right)_x\int_0^y \rho\left(\frac{u}{u_e}\right)\mathrm{d}y = \left(\mu\frac{\partial u}{\partial y}\right)_w - \mu\frac{\partial u}{\partial y}. \quad (14)$$

If there are defined new functions analogous to the displacement and momentum thickness in form but with their dependence on the transformed variable t retained, equation (14) becomes

$$\frac{1}{r}\frac{\mathrm{d}}{\mathrm{d}x}[\rho_e\mu_e u_e^2 r\Phi] + \rho_e\mu_e u_e u_{e_x}\Phi^* - \rho_e\mu_e u_e^2\tau\tau_{xt} = \mu_e[C(u_t)_w - Cu_t] \quad (15)$$

where

$$\Phi = \frac{u}{u_e}\int_0^t \frac{u}{u_e}\,\mathrm{d}t - \int_0^t\left(\frac{u}{u_e}\right)^2\mathrm{d}t \quad (16)$$

$$\Phi^* = \int_0^t \frac{h_s}{h_{s_e}}\,\mathrm{d}t - \frac{u}{u_e}\int_0^t \frac{u}{u_e}\,\mathrm{d}t \quad (17)$$

$$\tau = \int_0^t \frac{u}{u_e}\,\mathrm{d}t. \quad (18)$$

Now, if equation (15) is integrated from $t = 0$ to ∞, there results

$$\frac{\mathrm{d}\psi}{\mathrm{d}x} + \psi\frac{\mathrm{d}}{\mathrm{d}x}\ln(\rho_e\mu_e r) + \psi\frac{(\bar{H}+2)}{u_e}\frac{\mathrm{d}u_e}{\mathrm{d}x} - \int_0^\infty \tau\tau_{xt}\,\mathrm{d}t = \frac{\mu_{s_e}^2}{\rho_e\mu_e u_e}\int_0^\infty [(C\tau_{tt})_w - C\tau_{tt}]\,\mathrm{d}t \quad (19)$$

where

$$\psi = \int_0^\infty \Phi\,\mathrm{d}t \quad (20)$$

$$\psi^* = \int_0^\infty \Phi^*\,\mathrm{d}t \quad (21)$$

$$\bar{H} = \psi^*/\psi. \quad (22)$$

The new thickness ψ thus becomes equivalent to the moment of momentum in the transformed plane, x, t. As pointed out by Whitehead [22] for an incompressible flow, ψ represents the actual moment of momentum in the boundary layer and equation (19) is identical to that obtained if the original momentum equation were multiplied by the y co-ordinate and integrated directly. The quantity $\bar{H}$ was introduced as a modified form factor. The final equation in this form bears a resemblance to the von Kármán integral relation [equation (1)], except for the addition of one term. In performing the required integrations to obtain ψ, ψ^*, etc., it is noted that certain terms in the expressions diverge when evaluated at the upper limit of integration. If, however, these terms are grouped together, it will be observed that they disappear identically if the von Kármán integral relation is satisfied. It should also be noted that in the integral on the right-hand side of the equation, (the product of the density–viscosity ratio and the normal velocity derivative) can be integrated in closed form only if $n = 1{\cdot}0$. Since the value of n was set equal to $0{\cdot}7$ to be consistent with the results of [4], this integral was evaluated numerically in each step of the x-wise integration along the surface by using the values of the dependent variables existing at the preceding value of x. Owing to the relatively small x-wise variation of the variables K_1, K_2 and K_3 for the step size utilized, this method gives an accurate representation of this integral.

Using the profiles given by equations (7) and (8), therefore, one obtains the following non-dimensional equation from equation (19):

$$\frac{\mathrm{d}}{\mathrm{d}\bar{x}}(\bar{\lambda}^2) + \frac{a_5}{a_4}\bar{\lambda}^2\frac{\mathrm{d}K_1}{\mathrm{d}\bar{x}} = \frac{\bar{\lambda}^2}{a_4}\Big\{[a_6 - 4a_4 - (1-W)(1+2K_3+6K_2)]\frac{\mathrm{d}}{\mathrm{d}\bar{x}}\ln\bar{u} - 2a_4\frac{\mathrm{d}}{\mathrm{d}\bar{x}}\ln(\bar{\rho}\bar{\mu}\bar{r}) - \frac{I}{\bar{\rho}\bar{\mu}\bar{u}\bar{\lambda}^2}\Big\}. \quad (23)$$

The von Kármán integral relations for the momentum and the energy equations can also be reduced to a similar form and result in the following set of differential equations:

$$\frac{\mathrm{d}}{\mathrm{d}\bar{x}}(\bar{\lambda}^2) - \frac{2\bar{\lambda}^2}{\Gamma}(1+K_1)\frac{\mathrm{d}K_1}{\mathrm{d}\bar{x}} = \bar{\lambda}^2\left\{\frac{4W^{n-1}(1+K_1)}{\Gamma\bar{\rho}\bar{\mu}\bar{u}\bar{\lambda}^2} - 2\frac{\mathrm{d}}{\mathrm{d}\bar{x}}\ln(\bar{\rho}\bar{\mu}\bar{r}) - 2(H_c+2)\frac{\mathrm{d}}{\mathrm{d}\bar{x}}\ln\bar{u}\right\}, \quad (24)$$

$$\frac{\mathrm{d}}{\mathrm{d}\bar{x}}(\bar{\lambda}^2) + \frac{2\varphi_3}{\varphi_1}\bar{\lambda}^2\frac{\mathrm{d}K_1}{\mathrm{d}\bar{x}} + \frac{2\varphi_2}{\varphi_1}\bar{\lambda}^2\frac{\mathrm{d}K_3}{\mathrm{d}\bar{x}} = \frac{2W^{n-1}(1-K_3)}{\varphi_1\sigma\bar{\rho}\bar{\mu}\bar{u}} - 2\bar{\lambda}^2\frac{\mathrm{d}}{\mathrm{d}\bar{x}}\ln(\bar{\rho}\bar{\mu}\bar{u}\bar{r}). \quad (25)$$

A complete set of equations now exists for the determination of the boundary-layer characteristics downstream of a mass-transfer region. Equations (23–25) represent a set of simultaneous, first-order differential equations in the variables K_1, K_3 and λ. The initial values of these parameters are specified by the aforementioned conditions on the continuity of boundary-layer thickness, form factor and shape factor. The additional parameter in the enthalpy profile K_2 is related to the above variables by the energy equation evaluated at the wall [equation (13)]. Therefore, the equations can be solved by numerical integration by utilizing the method of [19] with the appropriate initial values. This integration was performed on the Bendix G-15 digital computer. Immediately downstream of the junction the step size used was extremely small ($\Delta\bar{x} = 0{\cdot}001$) owing to the large variation in boundary-layer characteristics that occurs there. This was increased gradually to a step size of 0·1 on the cylindrical portion of the body.

III. NUMERICAL COMPUTATIONS AND DISCUSSION OF RESULTS

As stated previously, the solution for a completely impermeable body was determined first to establish the applicability of the method. The analysis is now divided into two parts. The stagnation-point solution, which degenerates to the problem of four simultaneous algebraic equations, and the downstream region for which the differential equations must be solved. The heat-transfer results are presented in terms of a Nusselt number and Reynolds number based on stagnation conditions evaluated behind the normal shock. The form of this heat-transfer parameter permits extrapolation of the results over a wide range of stagnation temperature and pressure (cf. [23]).

Consider first the stagnation-point solution; there, the rate of change of all the integral thicknesses is equal to zero, resulting in the vanishing of the x-wise derivatives of the dependent variables. Therefore, the left-hand side of equations (23–25) drops out. The derivatives remaining in the right-hand side of these expressions can be evaluated directly, since in the stagnation region of a blunt body the velocity external to the boundary layer is a linear function of the surface co-ordinate and the radius can be replaced by the surface co-ordinate. The non-dimensional velocity gradient is given by

$$\bar{\beta} = \frac{\mathrm{d}\bar{u}}{\mathrm{d}\bar{x}} = (2\varphi_{s_e})^{\frac{1}{2}}$$

for a Newtonian pressure distribution. Therefore, equations (23–25) are reduced to algebraic equations which, in conjunction with equation (13), can be solved numerically for the four dependent variables. The results of the solution of this set of equations is presented in Fig. 1. For the Nusselt and Reynolds numbers defined by

$$N_{Nu} = \frac{q_w C p_{s_e} R_0}{(h_{s_e} - h_w)k_{s_e}}, \qquad \tilde{N}_R = \frac{\rho_{s_e}[h_{s_e}]^{\frac{1}{2}}R_0}{\mu_{s_e}}\varphi_{s_e}^{\frac{1}{2}},$$

the heat-transfer parameter in terms of the non-dimensional quantities enumerated above becomes

$$\frac{N_{Nu}}{\tilde{N}_R^{\frac{1}{2}}} = \frac{W^{n-1}(1-K_3)}{\varphi_{s_e}^{\frac{1}{2}}\bar{\lambda}}.$$

This parameter is plotted in Fig. 1 as a function of the ratio of wall to stagnation enthalpy. Also included for comparison are the integral-method results of [12], the cold-wall solution of [9] and the more accurate results of [15]. It is readily seen that the present analysis compares favorably with the results of [15] for $W > 0{\cdot}3$, while for a low wall temperature the two results diverge rapidly. At first glance this appears to be a major deficiency in the present

method; however, if the results are compared on a different basis the importance of this deviation appears to be slight.

The surface distribution of heat transfer with no injection was then obtained by utilizing the stagnation point values of the variables, K_1, K_2, K_3 and λ as initial values in the differential equations (23–25) governing the flow over the surface. The external flow properties were obtained from the experimentally determined pressure distribution of [23]. This corresponds to the flow at a free-stream Mach number of 6·0 over a hemisphere cylinder. The pressure distribution utilized is plotted in Fig. 2 as a function of the non-dimensional surface coordinate $\bar{x}$. Various values of the wall enthalpy ratio were chosen, the maximum being 1·35 for the heated-wall condition and the minimum being 0·1 which corresponds to the cold-wall case. These distributions are presented in Fig. 3 and compared with the cold-wall prediction of [9]. Since it has already been established that the stagnation-point value is not too accurate at low surface temperatures, the heat-transfer distributions are normalized with respect to the stagnation-point value. It is evident from Fig. 3 that the distribution is predicted fairly accurately even though the stagnation-point value is in error. It should also be noted that the predicted effect of wall temperature on the heat-transfer distribution is extremely small; this is substantiated by the experimental results of [17], for example, where values of W as high as 0·85 were obtained in the tests.

The downstream influence of mass transfer was then treated for the conditions corresponding to the experimental results of [23]. Therein, the injection region terminated at $\bar{x}_i = 0{\cdot}167$ and the ratio of wall to stagnation enthalpy W was equal to an average value of 0·35. The ratio of coolant to stagnation temperature θ_w was also approximately 0·35 in all the tests. In order to determine the initial values of the dependent variables, the boundary-layer thickness and integral thicknesses were obtained from the integral-method solution of [4]. These values are presented as a function of the non-dimensional injection parameter $(-f_w)$. The similarity parameter (N_1) permitting extrapolation of the heat-transfer results of a downstream-influence problem was obtained in [23] and is related to the mass-transfer rate by

$$N_1 \equiv \frac{m_c}{R_0 \mu_{s_e} \tilde{N}_{R^{\frac{1}{2}}}} = 2^{\frac{1}{2}}\pi(\bar{\rho}\bar{\mu})_i^{\frac{1}{2}}(1 - \cos\bar{x}_i)(-f_w). \quad (27)$$

Therefore, for a specified injection region, θ_w and W, the thicknesses can be obtained for any value of N_1. The initial values of the variables K_1, K_2, K_3 and λ are then obtained from the simultaneous solution of the algebraic equations (9–13). The results of the integration of the differential equations with the appropriate initial conditions are shown in Fig. 4 for $\theta_w = 0{\cdot}35$, $W = 0{\cdot}35$, and $\bar{x}_i = 0{\cdot}167$. There is obtained a large increase in heat transfer in the x-wise direction from $\bar{x} = \bar{x}_i$ and a peak local-heat transfer which decreases and moves downstream as the injection rate increases. This behavior is in qualitative agreement with the results of [23]. It should also be noted that there is a discontinuity in the heat-transfer rate at $\bar{x}_i$ (zero heat transfer is obtained on the porous region, from [4], for the high rates of injection considered here). This result was also obtained in the finite difference solution of [5]. In order to compare quantitatively these results with the experimental data of [23], it is more convenient to present the variation of heat transfer with mass transfer for a given surface location. This is shown in Fig. 5 for surface locations at which thermocouple data were available. As noted previously in the stagnation-point solution, there is a discrepancy in the heat-transfer level; however, the variation with mass transfer is predicted reasonably well.

Since the zero-injection, heat-transfer distribution is predicted fairly well by the present theory, and the effect of mass injection is also reasonably accurate, this suggests a method for determining the downstream influence of mass transfer. It consists of multiplying the heat-transfer rates, obtained from the present analysis, by the ratio of the stagnation-point prediction of [15] and the zero-injection stagnation-point value of the present analysis. This procedure provides a correction for the relatively inaccurate values of the stagnation-point heat transfer resulting at low wall temperatures.

To determine the effect of coolant temperature

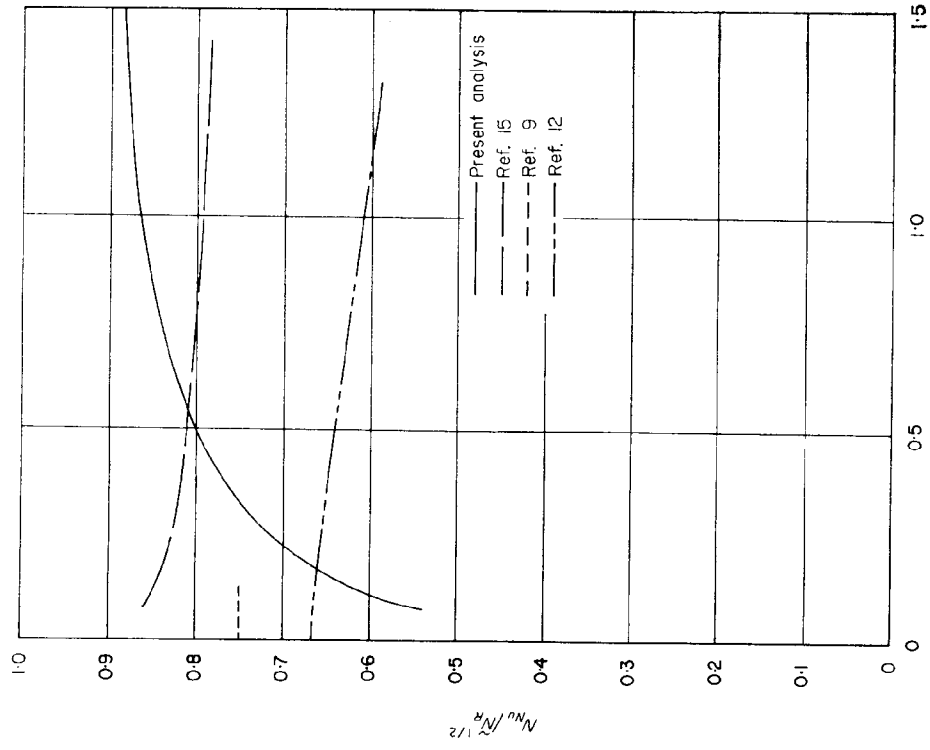

FIG. 1. Variation of stagnation-point heat transfer with wall temperature.

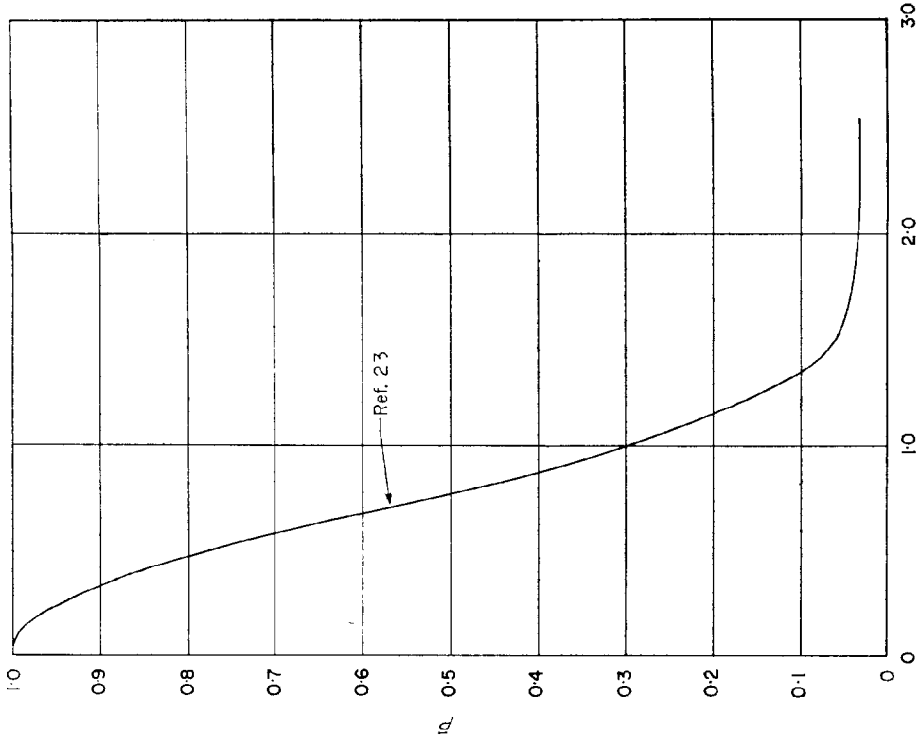

FIG. 2. Pressure distribution for hemisphere–cylinder ($M_\infty = 6{\cdot}0$).

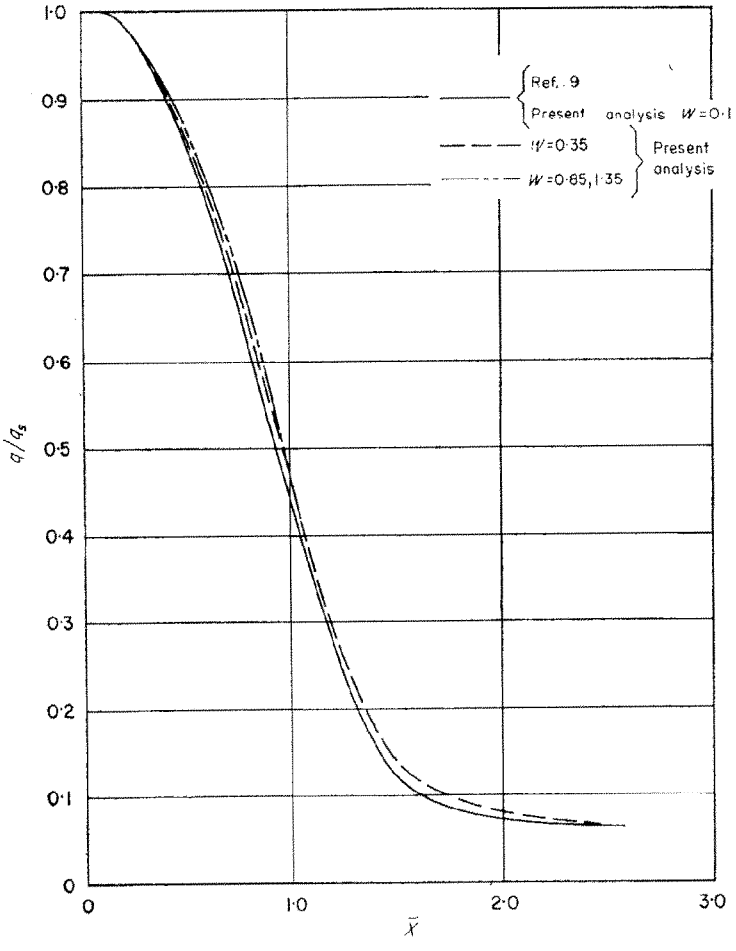

FIG. 3. Surface distribution of heat transfer for various wall temperatures.

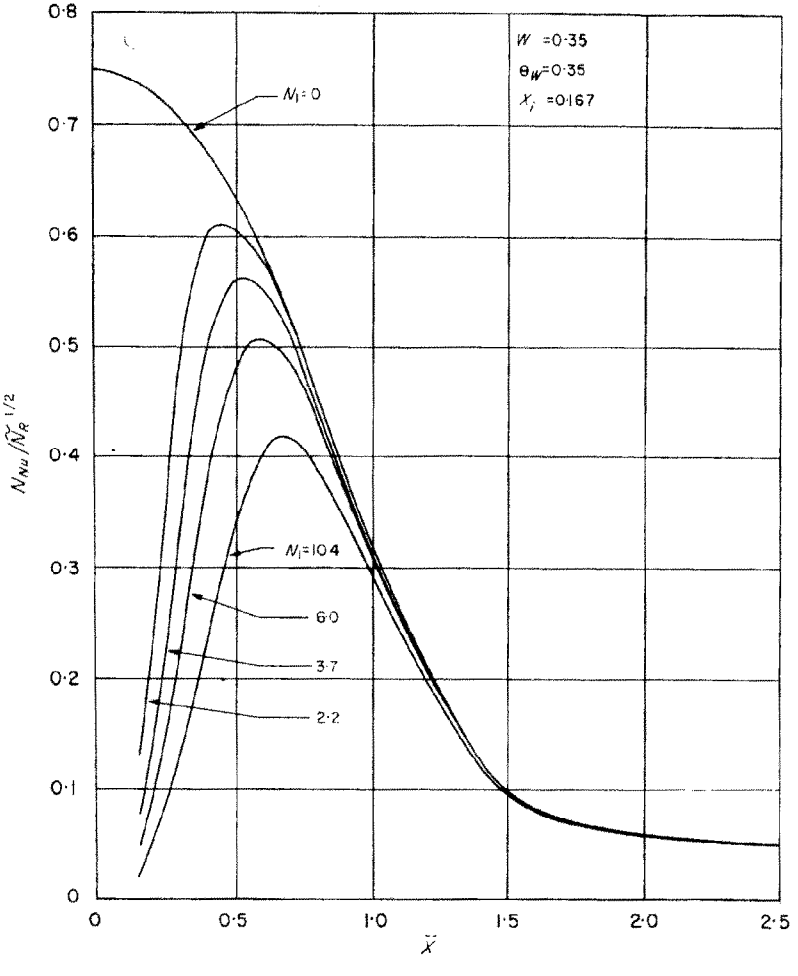

FIG. 4. Distribution of heat transfer for various injection rates.

on the heat-transfer characteristics, a calculation was performed with the same values of $\bar{x}_i$ and W but with different θ_w. The results for θ_w equal to 0·10 and 0·65 are presented in Figs. 6 (a) and (b), respectively. Comparison of these results with those of Fig. 4, $\theta_w = 0{\cdot}35$, indicates that the peak heat rate is decreased and moves downstream as the coolant temperature is decreased. This has the same effect as increasing the mass-transfer rate; for example, approximately the same heat-transfer distribution results from $N_1 = 10$ and $\theta_w = 0{\cdot}65$ as from $N_1 = 4$ and $\theta_w = 0{\cdot}1$. Both of these cases correspond to the same impermeable surface temperature ($W = 0{\cdot}35$).

The extent of the injection region can be varied by changing the value of $\bar{x}_i$. In addition to the model in which the porous region extended over a semivertex angle of approximately 9·5° ($\bar{x}_i = 0{\cdot}167$), there were also computed distributions corresponding to angles of approximately 20° ($\bar{x}_i = 0{\cdot}35$) and 29° ($\bar{x}_i = 0{\cdot}50$). These distributions are presented in Figs. 7 (a) and (b), respectively. It is evident that increasing the spatial extent of the injection region results in lower-peak heat-transfer rates as well as decreased over-all heat transfer to the surface. It should be noted that the over-all heat transfer is effected not only by the distribution for $\bar{x} > \bar{x}_i$, but is also due to the fact that for the relatively large injection rates considered, the heat transfer to the porous region is identically zero. A parameter that has been previously used (cf. [23]) to evaluate the over-all effectiveness of a given mass-transfer system is the effective enthalpy. This is denoted by Q and is defined as

$$Q \equiv \frac{1}{m_c}\int_0^{x_T} (q_{m_c=0} - q_{m_c})\,\mathrm{d}A. \qquad (28)$$

In terms of the non-dimensional, similarity parameters used herein, one obtains

$$\bar{Q} = \frac{2\pi h_{s_e}(1-W)}{N_1 \sigma_{s_e}} \int_0^{\bar{x}_T} \left[\left(\frac{N_{Nu}}{\bar{N}_R^{\frac{1}{2}}}\right)_{N_1=0} - \frac{N_{Nu}}{\bar{N}_R^{\frac{1}{2}}}\right] \bar{r}\,\mathrm{d}\bar{x}. \qquad (29)$$

The effective enthalpy has been computed for the conditions presented in Figs. 4, 6 and 7 and is presented in Figs. 8(a) and (b). Fig. 8(a) indicates the variation of effective enthalpy with coolant temperature, and Fig. 8(b) shows the effect of varying the injection area. It is seen that for the particular case when $W = 0{\cdot}35$ it is more advantageous to inject a very low-temperature fluid over a relatively small area than a fluid at the same temperature as the impermeable surface over a relatively large area. Both the total heat absorbed and the peak heating value are reduced for the same N_1, for example, if $\theta_w = 0{\cdot}1$ and $\bar{x}_i = 0{\cdot}167$ compared with $\theta_w = 0{\cdot}65$ and $\bar{x}_i = 0{\cdot}50$. As the impermeable surface temperature is decreased, however, the relative merits of decreasing the coolant temperature versus extending the injection region may be altered.

IV. CONCLUSIONS

The integral method has been applied to determine the downstream influence of mass transfer in the stagnation region of a blunt body. The analysis is performed utilizing exponential profiles for the velocity and stagnation enthalpy in the boundary layer. For the completely impermeable surface, results are obtained for both the "cold wall" condition and for a value of the ratio of wall to stagnation enthalpy greater than unity. The "cold wall" results are found to compare extremely well with those of [9]. The surface heat-transfer distribution was found to be practically unaffected by the variation in wall temperature; this has also been substantiated by experimental results.

For the analysis of the downstream effects, it was found that the specification of continuity of boundary-layer thickness, form factor and shape factor at the junction of the permeable and impermeable surface leads to consistent results over a wide range of mass-transfer rates and coolant temperatures. This specification provides the initial conditions for the three differential equations. The complete set of equations is solved numerically for various injection rates, coolant temperatures and injection areas. The profiles† resulting from this

† The computed values of K_1 vary between 0·3 and 1·0 for all the cases presented; examination of the assumed velocity profile indicates that positive values of K_1 correspond to $(u/u_e)_{\max} > 1{\cdot}0$; thus, the resulting profiles are non-monotonic.

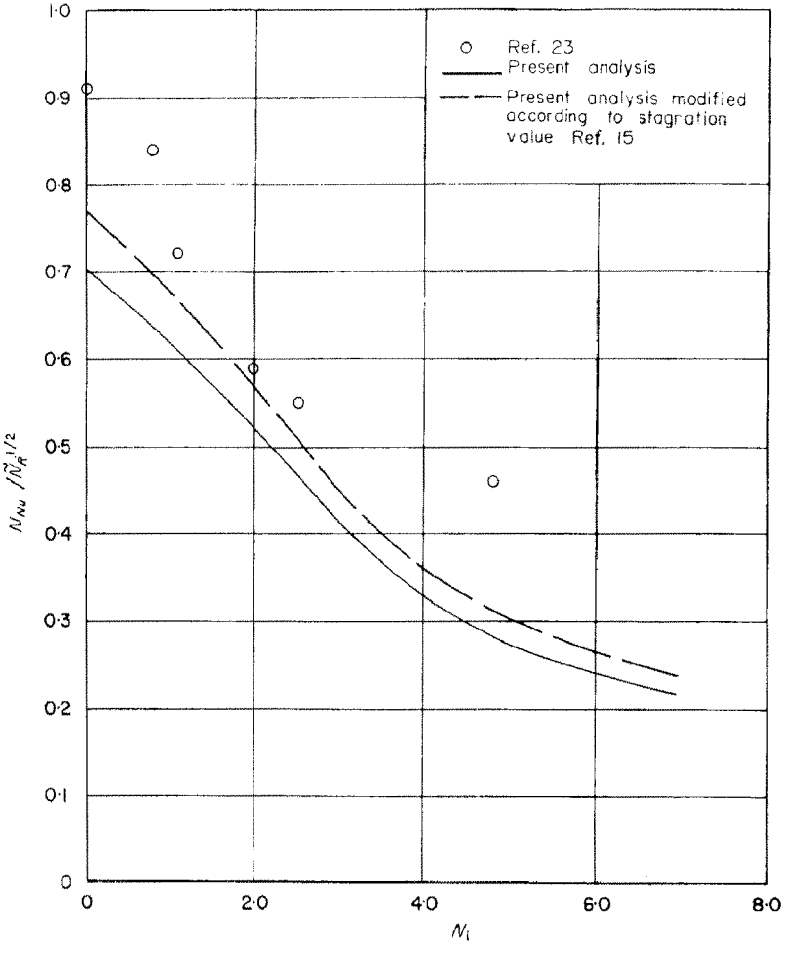

(a) $\bar{x} = 0{\cdot}33$

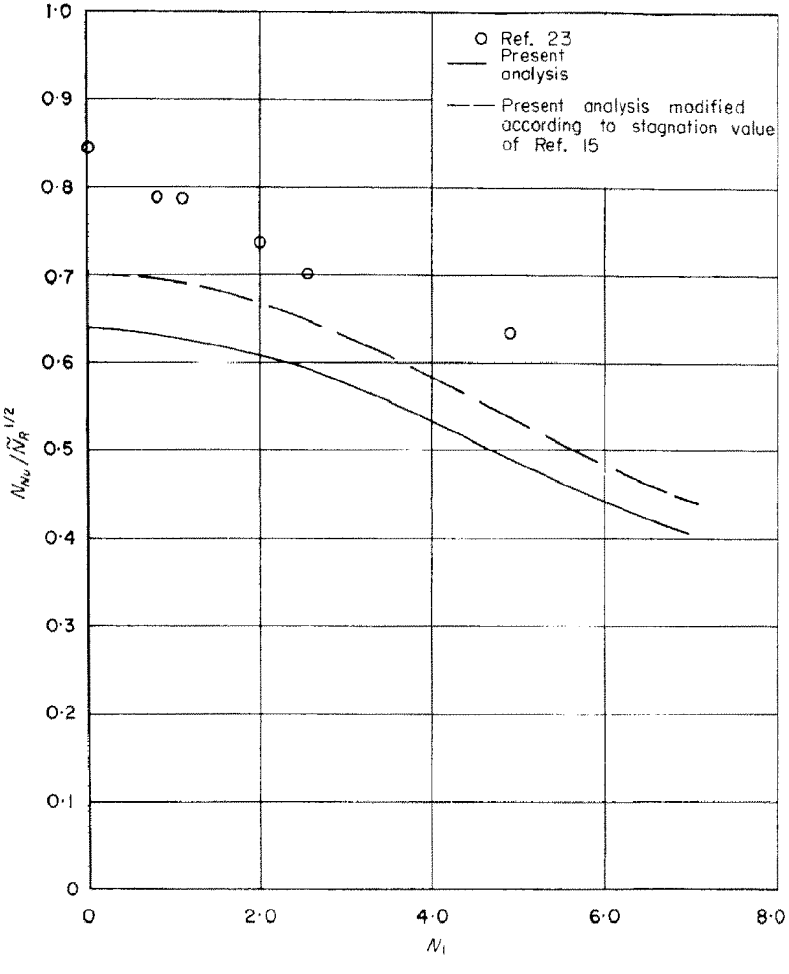

(b) $\bar{x} = 0{\cdot}50$

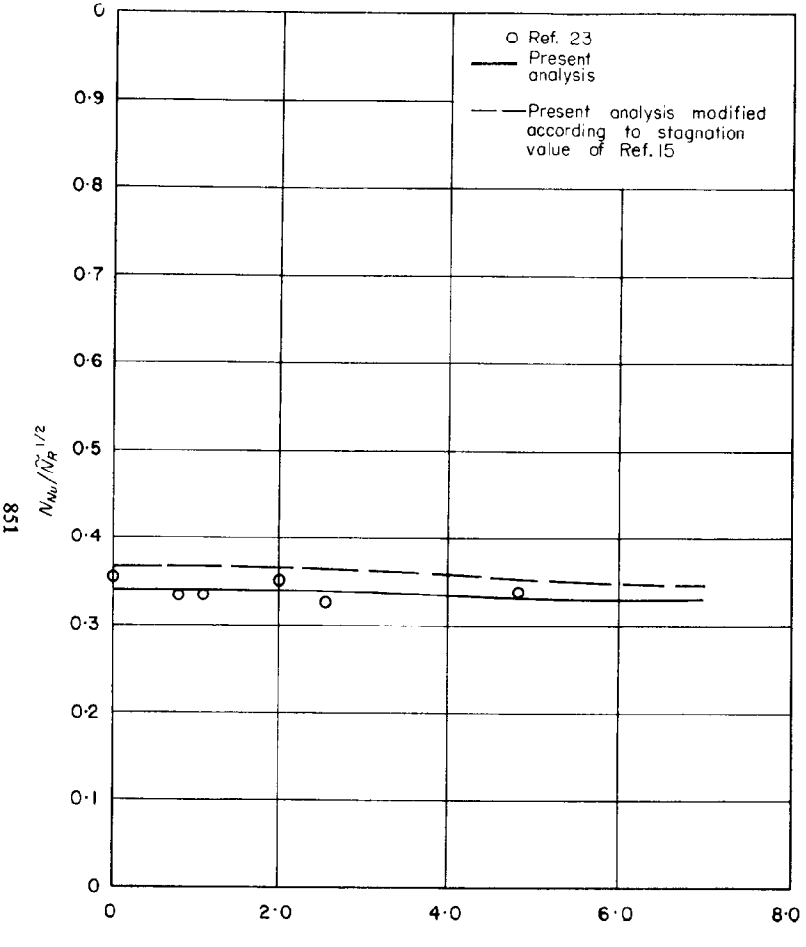

(c) $\bar{x} = 1{\cdot}0$

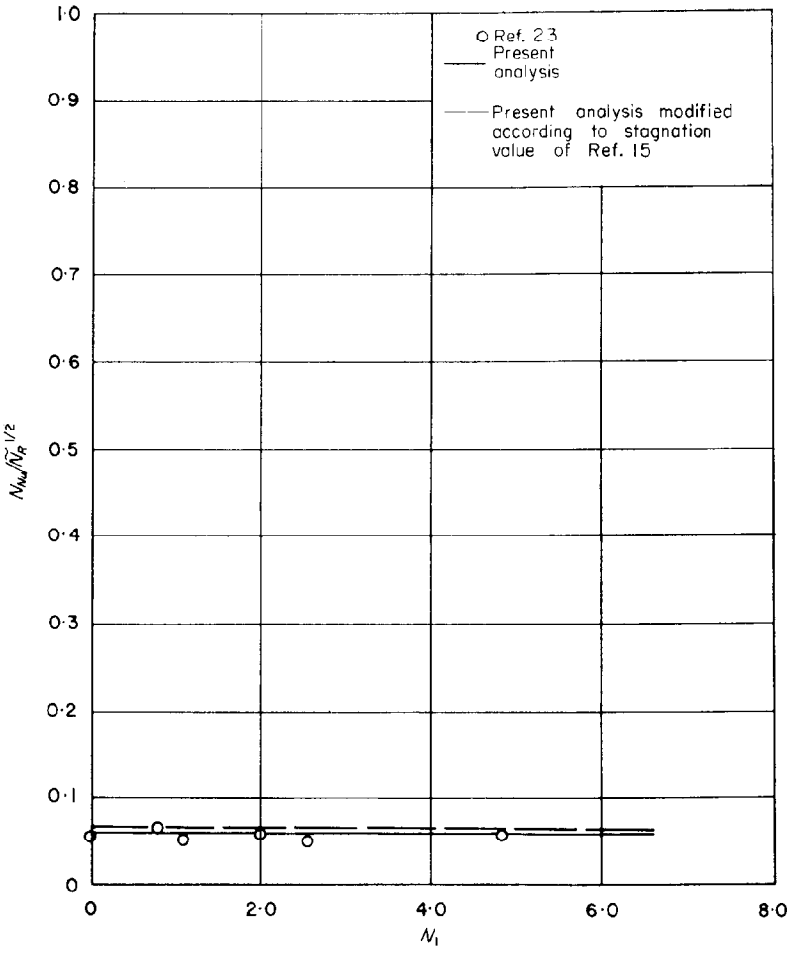

(d) $\bar{x} = 2{\cdot}0$

FIG. 5. Variation of heat transfer with mass transfer.

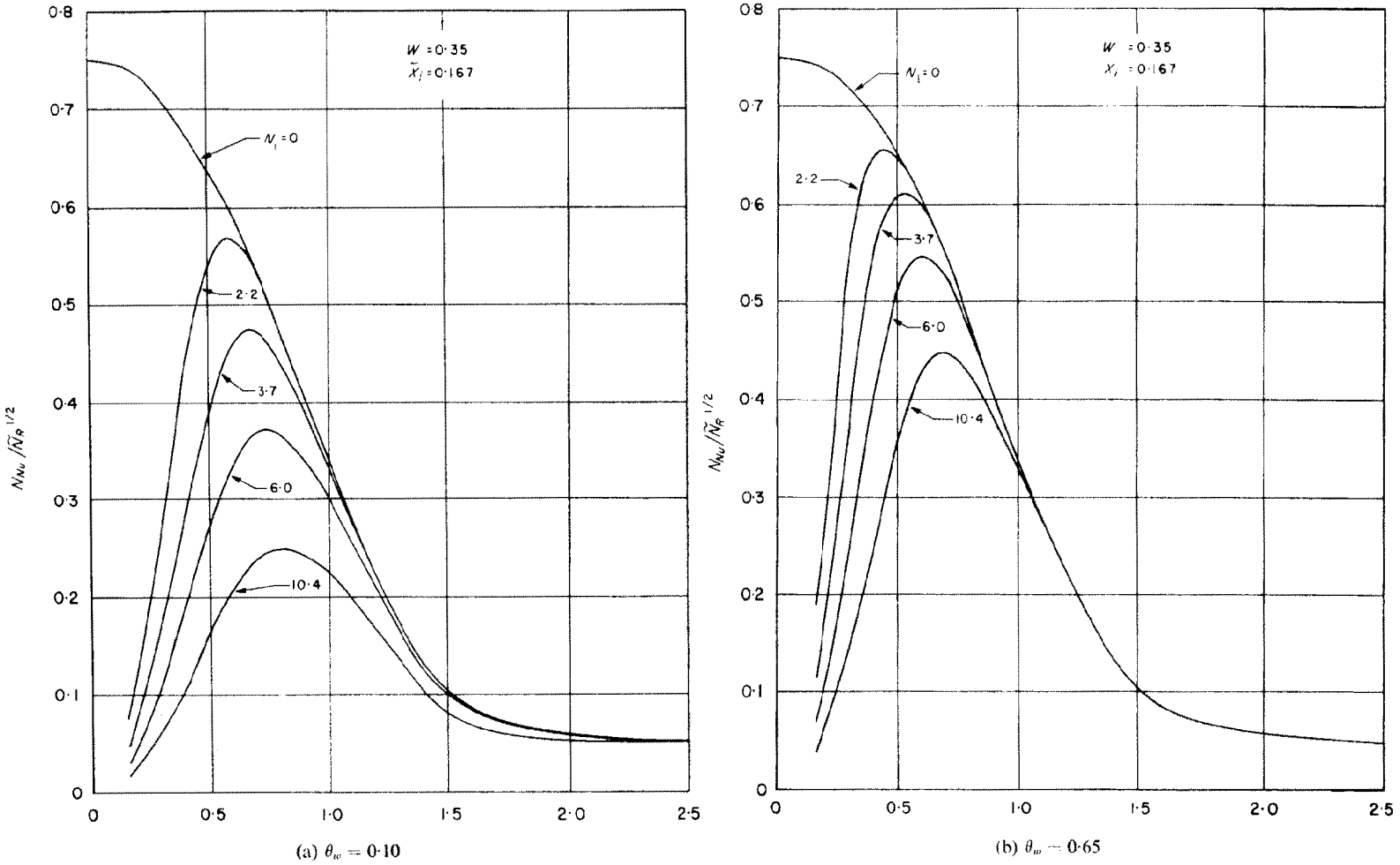

(a) $\theta_w = 0{\cdot}10$ (b) $\theta_w = 0{\cdot}65$

FIG. 6. Distribution of heat transfer for various injection rates.

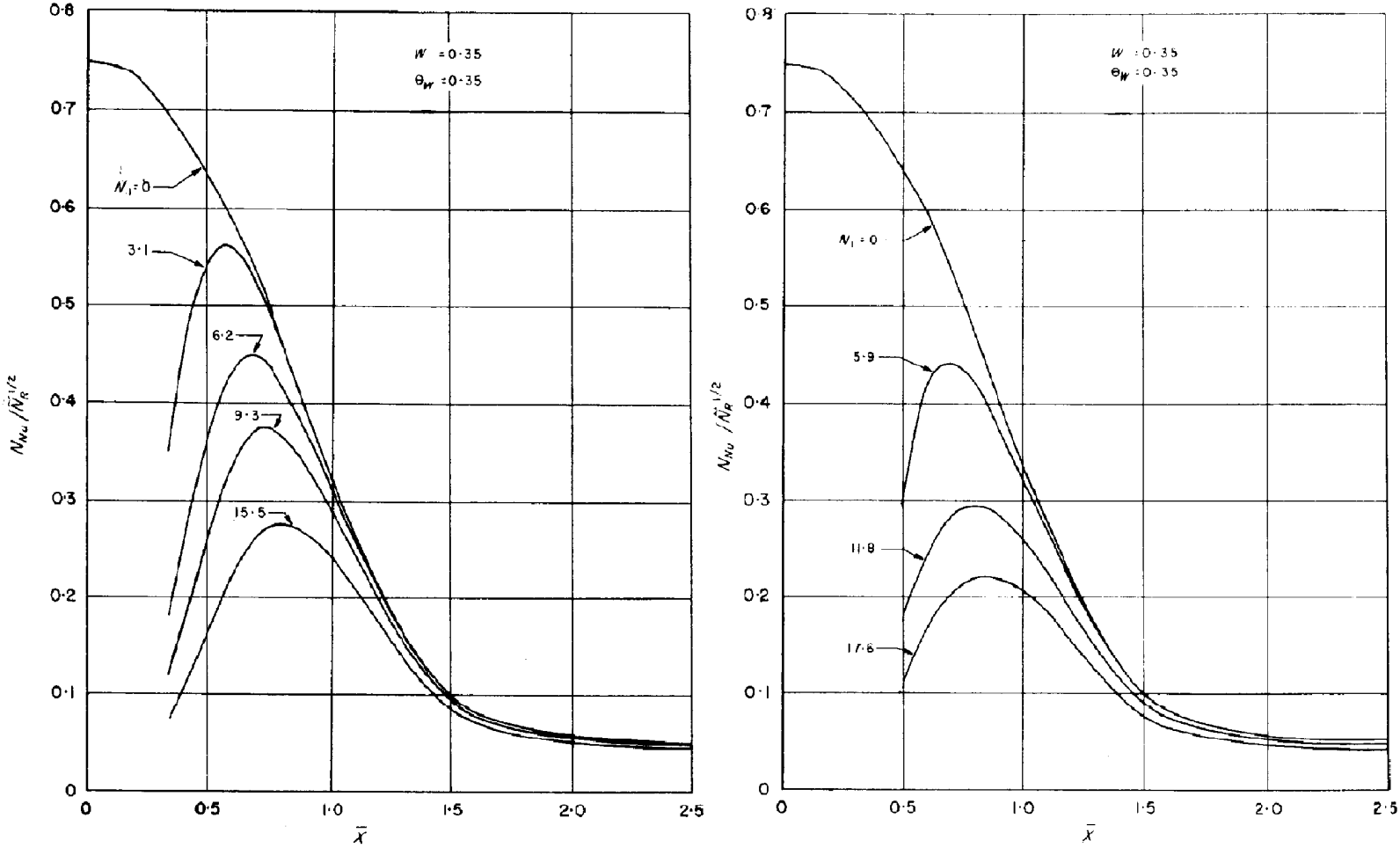

(a) $\bar{x}_s = 0{\cdot}35$ (b) $\bar{x}_s = 0{\cdot}5$

FIG. 7. Distribution of heat transfer for various injection rates.

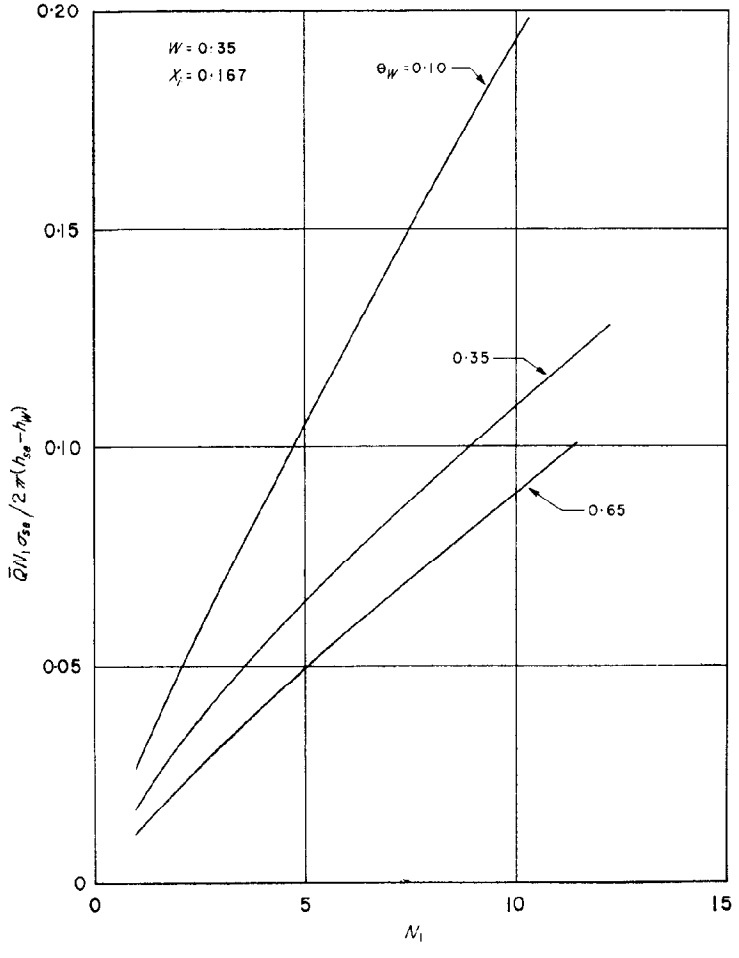

(a) Distribution of effective enthalpy with mass transfer for various coolant temperatures.

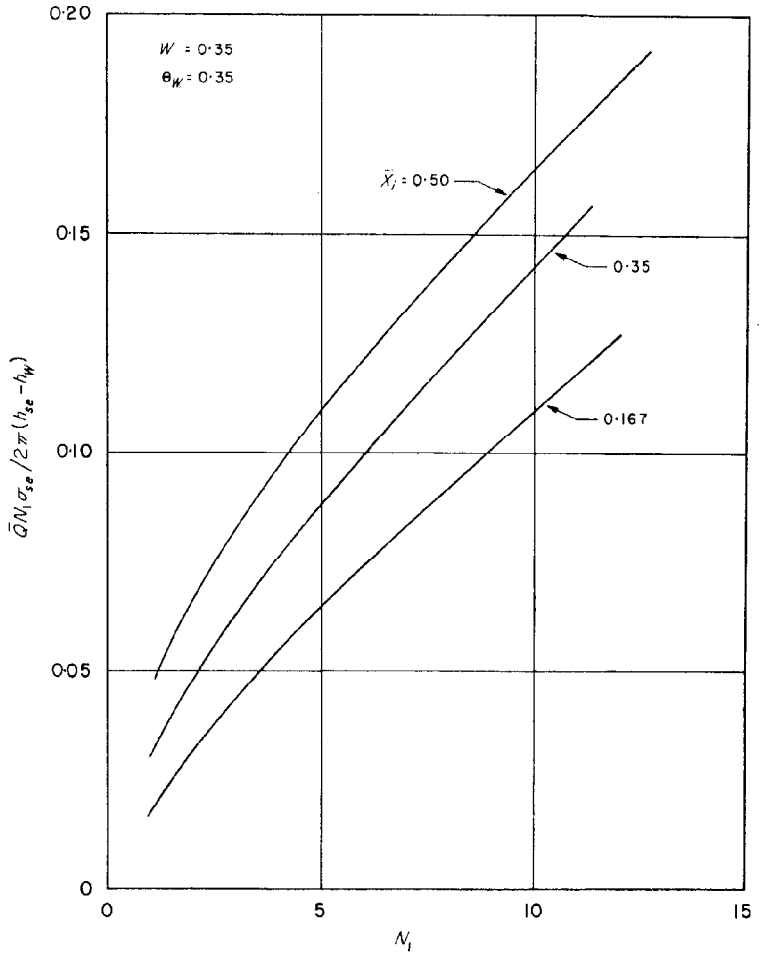

(b) Distribution of effective enthalpy with mass transfer for various injection areas.

FIG. 8.

analysis are found to exhibit the same behavior as indicated in [11], in which a non-monotonic variation of velocity in the boundary layer was obtained. In contradistinction to the analysis of [11], however, no singularities occur in the present solutions.

The results of the present analysis underestimate the heat-transfer rates for low wall temperature and overestimate them for high wall temperatures ($W > 0{\cdot}5$). The surface distribution of heat transfer for zero injection is predicted extremely well when normalized with respect to the stagnation-point value; similarly, the mass-transfer effects are predicted reasonably well when normalized with respect to the local zero-injection heat rate.

It was found, for the same total mass injected into the boundary layer, that either increasing the injection area or decreasing the coolant temperature results in lower-peak heat-transfer rates and a decrease in the total heat absorbed by the body.

ACKNOWLEDGEMENTS

This research was conducted under two contracts; the theoretical analysis was performed under USAF contract AF 33(616)-5944, administered under the direction of Materials Central, Wright Air Development Division, with Mr. Hyman Marcus acting as project engineer. The numerical computations were performed under Contract No. AF 33(616)-7661 administered by the Aeronautical Research Laboratory of the Air Research and Development Command, with Lt. John D. Anderson as the contract monitor.

The author is pleased to acknowledge the assistance of the computing staff of PIBAL in programming the equations for the Bendix G-15 digital computer and performing the numerical calculations, and also to express his gratitude to Professor Paul A. Libby for his helpful discussions and suggestions in the research discussed herein.

REFERENCES

1. M. MORDUCHOW, On heat transfer over a sweat-cooled surface in laminar compressible flow with a pressure gradient. *J. Aero. Sci.* **19**, 705–712 (1952).
2. J. N. B. LIVINGOOD and P. L. DONOUGHE, Summary of laminar-boundary-layer solutions for wedge-type flow over convection and transpiration-cooled surfaces. *NACA* TN 3588 (1955).
3. J. T. HOWE and W. A. MERSMAN, Solutions of the laminar compressible boundary layer equations with transpiration which are applicable to the stagnation regions of axisymmetric blunt bodies. *NASA* D-12 (1959).
4. P. A. LIBBY, The homogeneous boundary layer at an axisymmetric stagnation point with large rates of injection. Polytechnic Institute of Brooklyn, *PIBAL* Rep. No. 605, *WADD* TR 60-435 (1960); also *J. Aero. Space Sci.* **29**, 48–60 (1962).
5. J. T. HOWE, Some finite difference solutions of the laminar compressible boundary layer showing the effects of upstream transpiration cooling. *NASA* Memo 2-26-59A (1959).
6. P. A. LIBBY and A. PALLONE, A method for analysing the insulating properties of the laminar compressible boundary layer. *J. Aero. Sci.* **21**, 825–834 (1954).
7. M. W. RUBESIN and M. INOUYE, A theoretical study of the effect of upstream transpiration-cooling on the heat-transfer and skin-friction characteristics of a compressible boundary layer. *NACA* TN 3969 (1957).
8. P. M. CHUNG, Effect of localized mass transfer near the stagnation region of blunt bodies in hypersonic flight. *NASA* TN D-141 (1960).
9. L. LEES, Laminar heat transfer over blunt-nosed bodies at hypersonic flow speeds. *Jet Propulsion*, **26**, 259–269 (1956).
10. A. J. PALLONE, Non-similar solutions of the compressible laminar boundary layer equations with applications to the upstream transpiration cooling problem. Research and Advanced Development Div., AVCO Corp., *RAD* TR-9-60-8 (1960); also *J. Aero. Space Sci.* **28**, 449–456 (1961).
11. P. A. LIBBY and L. NAPOLITANO, A theoretical investigation of some boundary layer and heat transfer problems connected with hypersonic wind tunnel nozzles. Polytechnic Institute of Brooklyn, *AEDC* TR 55-51 (1955).
12. P. A. LIBBY, The laminar hypersonic heat transfer on blunt bodies according to the integral method. Polytechnic Institute of Brooklyn, *PIBAL* Rep. No. 398, paper presented at the 1958 Heat Transfer and Fluid Mechanics Institute at the University of California, Berkley, California (1958).
13. H. G. LEW, *On the Compressible Boundary Layer over a Flat Plate with Uniform Suction* (Reissner Anniversary Volume). Edwards, Ann Arbor (1949).
14. W. B. BROWN and J. N. B. LIVINGOOD, Solutions of laminar boundary-layer equations which result in specific-weight-flow profiles locally exceeding free-stream values. *NACA* TN 2800 (1952).
15. J. A. FAY and F. R. RIDDELL, Theory of stagnation point heat transfer in dissociated air. *J. Aero. Sci.* **25**, 73–85, 121 (1958).
16. N. H. KEMP, P. H. ROSE and R. W. DETRA, Laminar heat transfer around blunt bodies in dissociated air. *J. Aero. Sci.* **26**, 421–430 (1959).
17. R. J. CRESCI, D. A. MACKENZIE and P. A. LIBBY, An investigation of laminar, transitional and turbulent heat transfer on blunt-nosed bodies in hypersonic flow. Polytechnic Institute of Brooklyn, *PIBAL* Rep. No. 466, *WADC* TN 59-119, AD 214 617 (1959); also *J. Aero. Space Sci.* **27**, 401–414 (1960).
18. V. ZAKKAY, Laminar heat transfer and pressure

measurements over blunt-nosed cones at large angle of attack. *J. Aero. Sci.* **25**, 794–795 (1958).
19. S. GILL, A process for the step-by-step integration of differential equations in an automatic digital computing machine. *Proc. Camb. Phil. Soc.* **47**, 96–108 (1951).
20. W. B. BROWN and P. L. DONOUGHE, Tables of exact laminar boundary layer solutions when the wall is porous and fluid properties are variable. *NACA* TN 2479 (1951).
21. P. A. LIBBY, M. MORDUCHOW and M. H. BLOOM, Critical study of integral methods in compressible laminar boundary layers. *NACA* TN 2655 (1952).
22. L. G. WHITEHEAD, An integral relationship for boundary layer flow. *Aircr. Engng*, **21** (1949).
23. P. A. LIBBY and R. J. CRESCI, Experimental investigation of the downstream influence of stagnation point mass transfer. Polytechnic Institute of Brooklyn, *PIBAL* Rep. No. 520, *WADC* TN 59-210 (1959); also *J. Aero. Space Sci.* **28**, 52–64 (1961).

Résumé—La méthode intégrale est appliquée pour déterminer l'influence aval d'un transport de masse homogène dans la région d'arrêt d'un corps de révolution émoussé placé dans les conditions d'un vol hypersonique. On utilise les profils exponentiels pour essayer d'éliminer les singularités qui se sont révélées dans les études précédentes avec les profils en forme de polynomes. L'étude est améliorée par l'introduction d'une équation différentielle supplémentaire, obtenue par une seconde intégration de l'équation de quantité de mouvement. Quand on utilise cette dernière avec les relations intégrales de Kármán pour l'énergie et la quantité de mouvement, il en résulte des équations différentielles du premier ordre que l'on résoud par des méthodes numériques sur une calculatrice. Les conditions d'égalité à la limite de la surface perméable-imperméable fournissent les conditions initiales pour l'intégration.

Les résultats indiquent que les singularités qui interviennent dans l'application de la méthode intégrale utilisant des profils en forme de polynomes n'apparaissent pas dans cette étude. Les taux de transfert de chaleur obtenus sont comparés au données expérimentales et l'on trouve qu' ils traduisent assez bien l'influence aval d'une injection de masse. L'effet, sur les taux de transfert de chaleur, de la variation de température du refroidisseur et de la surface d'injection est également étudié. On trouve que la diminution de la température du refroidisseur ou l'accroissement de la surface d'injection se traduit par une diminution du flux de chaleur maximum et de la chaleur totale transmise au corps.

Zusammenfassung—Mit Hilfe der Integralmethode liess sich der Einfluss des homogenen Stoffüberganges im Staubereich eines stumpfen, achssymmetrischen Körpers bei Hyperschallgeschwindigkeit auf stromabwärts auftretende Vorgänge bestimmen. Um die bei Polynomprofilen früherer Analysen auftretenden Singularitäten zu vermeiden, wurden versuchsweise Exponentialprofile verwendet. Die Analyse erfolgte mit einer zusätzlichen Differentialgleichung, die sich aus der zweiten Integration der Bewegungsgleichung ergab. In Verbindung mit den Kármánschen Integralbeziehungen für die Bewegungs- und Energiegleichungen ergibt sich ein System von Differentialgleichungen erster Ordnung, das auf einer Digitalrechenmaschine numerisch lösbar ist. Übereinstimmende Bedingungen an der Grenze durchlässige-undurchlässige Oberfläche liefern die Anfangsbedingungen für die Integration.

Die Ergebnisse zeigen, dass die mit Polynomprofilen bei der Integralmethode auftretenden Singularitäten in der hier durchgeführten Analyse nicht in Erscheinung treten. Die ermittelten Daten für den Wärmeübergang werden mit experimentellen Ergebnissen verglichen und ermöglichen verhältnismässig gute Aussagen über stromabwärts auftretende Effekte bei Stoffzugabe. Der Einfluss verschiedener Kühlmitteltemperaturen und Stoffzugabeflächen auf den Wärmeübergang wurde ebenfalls untersucht. Eine Verkleinerung der Kühlmitteltemperatur oder Vergrösserung der Zugabefläche führt zu einer Abnahme der Wärmeübergangsspitzen und der dem Körper insgesamt zugeführten Wärmemenge.

Аннотация—В статье применяется интегральный метод для определения влияния однородного переноса массы в окрестности критической точки осесимметричного тела с тупой носовой частью в условиях гиперзвукового полета. Принимается экспоненциальный профиль для учета некоторых особенностей, возникших в предыдущих решениях, когда использовались полиномиальные профили. Анализ выполнен путем вывода дополнительного дифференциального уравнения, полученного вторичным интегрированием уравнения количества движения. Это уравнение вместе с интегральными соотношениями Кармана для уравнения количества количества движения и энергии дает систему дифференциальных уравнений первого порядка, которые решаются численно на цифровом счетно-решающем приборе. Условия на границе проницаемой и непроницаемой поверхностей являются начальными условиями для интегрирования.

Результаты показывают, что в данном анализе не возникают те особенности, которые

получаются при применении интегрального метода с использованием полиномиальных профилей.

Сделано сравнение полученных значений интенсивности теплообмена с экспериментальными и найдено, что они дают возможность достаточно хорошо определить влияние по направлению потока подвода массы. Проведено также исследование влияния температуры охладителя и области ввода массы на интенсивность теплообмена. Найдено, что понижение температуры охладителя или увеличение области ввода массы понижают максимальную скорость теплообмена, а также общее количество тепла, передоваемое телу.